27.5 W/m2 collection efficiency solar laser using a diffuse scattering cooling liquid

Smyth, Conor; Mirkhanov, Shamil; Quarterman, Adrian; Wilcox, Keith

Published in:
Applied Optics

DOI:
10.1364/AO.57.004008

Publication date:
2018

applied optics

27.5 W/m^2 collection efficiency solar laser using a diffuse scattering cooling liquid

C. J. C. Smyth,* S. Mirkhanov, A. H. Quarterman, and K. G. Wilcox

School of Science Maths and Engineering, University of Dundee, Dundee DD1 4HN, UK
**Corresponding author: C.Z.Smyth@dundee.ac.uk*

Received 15 February 2018; revised 4 April 2018; accepted 5 April 2018; posted 6 April 2018 (Doc. ID 323328); published 11 May 2018

We report a solar pumped solid state laser using a 20 mm long, 3 mm diameter neodymium-doped yttrium aluminum garnet laser rod. This rod was placed in a liquid cooling chamber using a water–white-emulsion-paint mix. This mix provides cooling for the laser crystal and also doubles as a diffuse light scattering liquid. This enhances sunlight scattering and leads to a greater absorption in the laser rod. We numerically model the solar absorption in the laser rod using a ray-tracing model and predict a 2.6 times enhancement in absorption when a 98% reflective diffuse scatter is modelled compared to 0% scattering. We experimentally demonstrated this, showing a 2.58 times increase in average output power of the solar laser compared to the use of pure water as a cooling liquid. Using the water–white-paint scattering cooling liquid, we demonstrated a laser with an output power of 2.3 W and with a collection efficiency of 27.5 W/m^2.

OCIS codes: (140.3460) Lasers; (140.3530) Lasers, neodymium; (350.6050) Solar energy.
https://doi.org/10.1364/AO.57.004008

1. INTRODUCTION

Since solar lasers were first demonstrated in 1966 [1], there has been steady progress made on improving their performance, in particular, their collection efficiency, which is the laser output power per square meter of primary sunlight concentrator. Currently, collection efficiencies of 31.5 W/m^2 have been achieved [2], and the typical route of development has involved increasing complexity of the solar concentration systems used to provide these efficiency gains [3–8]. In this work, we use a different approach not applied in solar laser technology before, based on a diffuse pump cavity. Diffuse pump cavities have been widely used for many years in flash lamp pumped neodymium-doped yttrium aluminum garnet (Nd:YAG) lasers to provide uniform pump distributions and to increase absorption [9–11]. We combine the functionality of the diffuse pump reflector and cooling by using a water–white-emulsion-paint mixture, which we flow around the outside of the laser rod. Furthermore, this approach of using a diffuse reflective pump cavity is potentially well suited to the implementation of wavelength conversion systems by adding luminescent converters, such as dyes or colloidal quantum dots [12], which could significantly increase the performance of solar solid state lasers.

It is possible to both side pump and end pump a solar laser [3–8] with both geometries carrying their individual benefits and setbacks. End pumping of a laser crystal rod provides better circularly symmetric homogeneity of absorbed light, however, it is limited by the length of the rod. Side pumping, on the other hand, is more scalable. Other less traditional geometries have also been used in the development of solar lasers, such as a solar pumped fiber [13] and solar pumped lasers through radiative energy transfer [12]. Other novel laser geometries, such as evanescent coupling, might offer the promise of a lower threshold [14], however, it would need additional modelling to determine their practicality.

Traditionally, flash lamp pumping of a laser crystal rod in a diffuse light chamber takes on a side pumped geometry with the flash lamp being placed within the diffuse light chamber alongside the laser medium. Side pumping, however, would not be an effective geometry in this solar laser setup, as our source of pump light is not contained in the diffuse light chamber, but is created externally from concentrated solar radiation. This would mean that a side pumped solar laser using a diffuse pump cavity would require a chamber with a section of the side of the laser rod exposed to the external incoming light. This, in turn, would result in higher losses of non-absorbed light and would greatly reduce the effectiveness of the diffuse reflective chamber. It is for these reasons that an end pumped geometry was selected for this work.

We undertake ray-tracing modelling of our solar laser system and show that the absorption of the solar spectrum by the Nd:YAG rod is increased by a factor of 2.6 when a 98% reflectivity diffuse scatterer is modelled around the rod in place of 0% scattering.

When this is incorporated into a four-level model of our laser, we predict an increase in slope efficiency from 4.7% to 11.0%. We experimentally implement this solar laser using a single stage solar concentrator based on a 40 cm × 40 cm Fresnel lens. We reach a maximum output power of 2.3 W with a collection efficiency of 27.5 W/m^2 using the water–white-paint cooling liquid and 0.89 W, 10.9 W/m^2 using pure water as our cooling liquid.

2. MODEL

We model our solar laser using ray tracing implemented in Matlab. The three-dimensional model generates a user-defined number of rays, each with a random wavelength, position, and incident angle at the input face of the laser rod. We set the range of allowed positions to match our 3 mm crystal end face diameter. The angle of the incident rays is set between normal incidence and 42.3°, which corresponds to the maximum angle of incident light we get from the Fresnel lens we use during the experiments. The wavelength of each ray is randomly assigned with a probability weighted to a standard AM1.5 solar spectrum (IEC 60904-3). The model traces each ray's path with a probability of absorption in the laser rod based on the absorption spectrum of 1.1% doped Nd:YAG [15] and a Lambert–Beer exponential absorption profile to provide an absorption position. When a ray reaches an end face of the crystal, it has a probability of being reflected or transmitted based on the Fresnel reflections (see Fig. 1). We initially allowed a gap between the rod side walls and the diffuse scatterer, but the model indicated that having zero gap produced the highest absorption. We, therefore, simplified the model to remove this gap so that when a ray hits an interface at the side of the rod it has a probability of being absorbed or scattered in a random direction weighted by Lambertian scattering.

Initially, we studied the effect of scattering medium reflectivity on total absorption in the rod, which is shown in Fig. 2. We find that the absorption increases significantly with increasing reflectivity, reaching nearly 25% at 98% reflectivity, which is taken as a maximum achievable value, for example, using barium sulphate coatings. Second, we investigated the absorption as a function of the incoming ray angle for a 0% and 98% diffuse reflector. This is shown in Fig. 2 in the inset. We show that with no diffuse reflector surrounding the rod, the absorption decreases rapidly as a function of the increasing input angle. This can be understood to arise from the path length of high angle rays in the rod being significantly shorter than those for low angle rays. On the other hand, when the 98% reflectivity scatterer is present, the absorption is enhanced across all angles with the maximum increase at angles around 10°. Rays at 0° incidence represent those that travel straight through the length of the crystal rod without interacting with the side surfaces. As the angle is increased, so too is the probability of interaction with the side surface of the laser rod, resulting in diffuse reflection from the chamber and, therefore, a longer path length through the laser medium up to this peak around 10°. This peak corresponds to rays of light on trajectories that hit the scattering liquid (the sides of the laser crystal rod) half-way down its 20 mm length. These rays, as a result of the diffuse reflector, have the highest potential for the longest path length through the laser medium and, therefore, have the highest potential for absorption. After this point, as the incoming ray angle is increased further, the probability of loss through the front surface of the crystal increases, and, therefore, these rays on average have shorter path lengths, reducing the probability of absorption. This is not the case with 0% reflectivity, as rays hitting the sides of the laser medium are not scattered but are lost. The higher the input angle in this case, the shorter the path length of the ray in the laser medium tends to be, which,

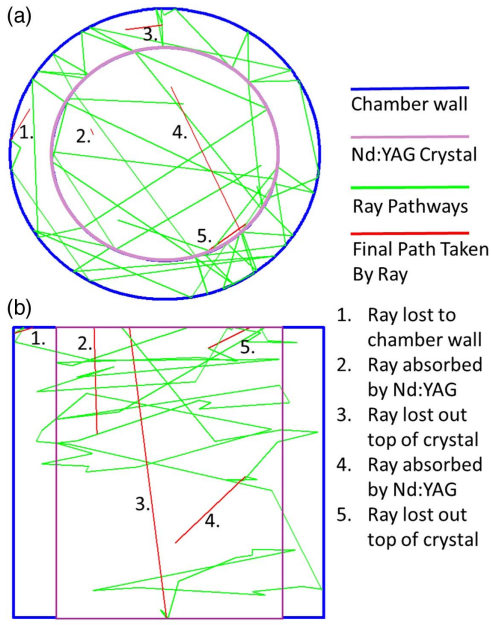

Fig. 1. Two-dimensional (2D) example of the ray-tracing computer model [(a) from top, looking down through model and (b) from side on, looking through the mode]. Rays are generated on the top surface of the figures and travel through the model. In this example five rays were used. Their pathways through the model are represented as green lines with the red lines indicating their final pass (either being absorbed or lost at this point).

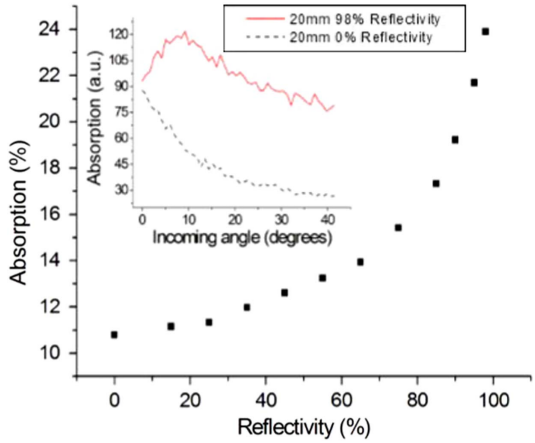

Fig. 2. Modelled solar absorption in the Nd:YAG rod as a function of reflectivity of the diffuse scatterer in contact with the side wall of the rod. The absorption as a function of the ray incident angle for 98% (red) and 0% (black) diffuse reflectivity is shown in the inset.

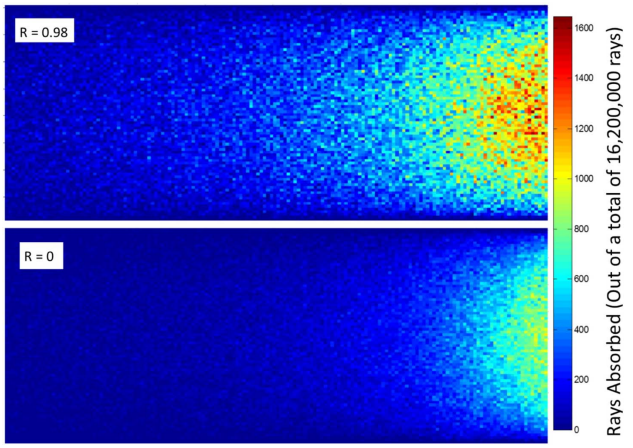

Fig. 3. Modelled solar absorption distribution in the 20 mm long, 3 mm wide Nd:YAG rod with a 98% diffuse reflector surrounding the rod (top) and 0% reflectivity (bottom). Light is input from the right.

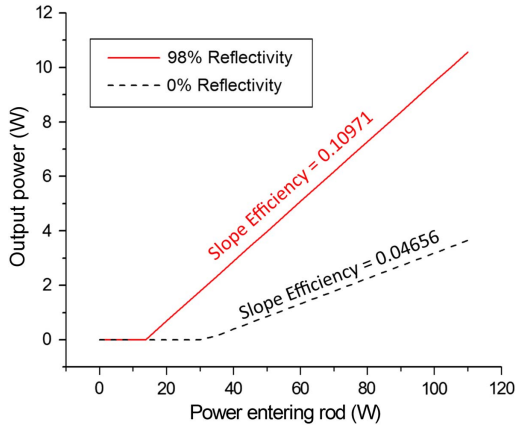

Fig. 4. Modelled laser output power as a function of solar power entering the 20 mm long, 3 mm diameter Nd:YAG rod for 98% reflectivity scatterer (red line) and 0% diffuse scatterer (black line).

in turn, reduces the chance of absorption. The diffuse reflector increases the absorption of higher angle rays, which correspond to a large fraction of the incoming sunlight from high solar concentration systems. We also investigated the effect of the initial position of the ray on the laser rod face for absorbed rays but found only a weak effect.

A cross section through the center of the laser rod showing the modelled absorption distribution with the 98% and 0% reflectivity scatterers surrounding the rod is shown in Fig. 3. Both the absorption and the homogeneity of the absorption are significantly increased when the 98% diffuse sunlight scatterer is used. We model the total absorption to be 9.46% with 0% diffuse scattering and 24.29% with 98% diffuse scattering in this configuration.

To model laser performance, we take the total absorption in the Nd:YAG rod calculated from the ray-tracing model and use this as an input for a standard four-level laser model based on Nd:YAG material properties [10]. We assume that all of the absorbed photons contribute to the laser level equally and that the laser mode overlap with the laser rod is one, as the implementation of the solar laser is expected to be highly multimode. We set output coupling losses to 2% to match the experimentally measured optimum, and other losses to 0.33%, which were measured using a Findley–Clay analysis of our solar laser [10]. The predicted laser power curves with respect to solar power entering the laser rod with 98% and 0% reflectivity diffuse scattering material are shown in Fig. 4.

3. EXPERIMENT

Experiments were performed between the 9th and 13th December 2016 on Tenerife at a latitude of 28.3° North. The conditions were cloud free and clear with direct solar intensities between 900 and 1050 W/m^2 during the experiments.

We experimentally implement our solar laser using a solar tracking telescope mount, on which we place our primary collector and laser. A schematic of the laser cavity and a photograph of the operating laser are shown in Figs. 5(a) and 5(b), respectively. The primary collector was a square plastic Fresnel lens with dimensions 40 cm × 40 cm and a focal length of 22 cm. No additional solar concentration was used. We noted that light from the corners of the lens were not affecting laser performance, so we added right angled triangles with edge dimensions of 10 cm, masking off each corner, giving an octagonal primary concentrator area of 0.114 m^2. The incident solar power was controlled using a series of shades placed in front of the Fresnel lens, each shading differing numbers of 1.9 cm wide stripes on the Fresnel lens.

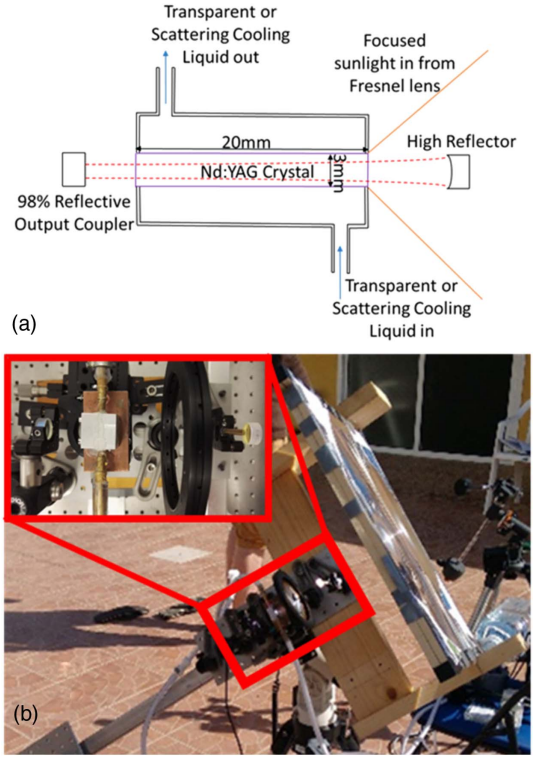

Fig. 5. (a) Schematic of the laser cavity, Nd:YAG rod, and cooling/scattering liquid chamber. (b) Photograph of the experimental solar laser in operation. The inset and red box correspond to the parts of the laser shown in part (a).

The front face of the antireflection (AR)/AR coated, 1.1% doped, 20 mm length, 3 mm diameter Nd:YAG rod was located at the focus of the Fresnel lens. The rod was mounted in an aluminium chamber, through which cooling liquid was pumped in a closed loop with total volume ~100 ml. Heat was then extracted from this closed loop using a forced air radiator heat exchanger. When pure water is used, the diffuse reflectivity of the chamber is low. To produce a highly scattering pump reflector in contact with the outside of the rod, the pure water was replaced with an approximately 1:1 mix of water and commercially available Dulux white emulsion paint in the closed loop. The laser cavity was formed between a curved high reflector with a radius of curvature 300 mm and a plane output coupler. The total cavity length was approximately 130 mm. Output couplings of 0.5%, 1%, 2%, and 5% transmission were tested with lasing achieved in all but the 5% transmission case and with the 2% output coupler being closest to optimal for our system. The laser output power was measured using a Thorlabs S146C power meter, and the solar irradiance was measured using a calibrated solar irradiance meter (Isotech ISM400) for each data set. The laser spectrum was recorded using a Stellarnet Greenwave spectrometer sensitive from 350 to 1180 nm with 2.8 nm FWHM resolution.

The measured solar laser power as a function of solar power incident of the front of the Fresnel lens are shown in Fig. 6 for both pure water and the paint–water mix. We obtain a maximum output power of 0.89 W with a threshold of 51 W and a slope efficiency of $1.3 \pm 0.1\%$ at an irradiance of 1010 W/m^2 in the case of pure water. A maximum output power of 2.3 W with a threshold of 45 W and a slope efficiency of $3.3 \pm 0.2\%$ at an irradiance of 927 W/m^2 for the water–paint mix. The collection efficiencies based on the full area of the primary concentrator were 7.7 W/m^2 and 20.0 W/m^2, respectively. This represents an increase in output power by a factor of 2.58 when the white-paint/water mix is used compared to water. There was no degradation of laser over time observed with both water and the water–white-paint solution. The stability of the lasers, however, was predominantly limited by clouds and, to a lesser extent, the accuracy of our tracking mount. Heat is extracted from the water–paint cooling liquid by a commercial computer processor cooling system. Therefore, the temperature of the liquid is kept stable with only small increases in temperature experienced under operation. We experimentally observed no degradation nor foresee substantial issues with degradation of the Delux white emulsion paint due to exposure to high temperatures, as these are not experienced in our system. However, should this prove to not be the case, a reliable substitution can be made of barium sulphate instead of the white emulsion paint. This, in theory, should provide a marginally higher level of diffuse reflectivity and has been used previously in diffuse light chambers of high powered lasers, where high temperatures are experienced [16]. The reason for using white emulsion paint in these experiments was due to availability, cost, and the ease at which it dilutes itself in water. These are valuable features during research on solar lasers in the field.

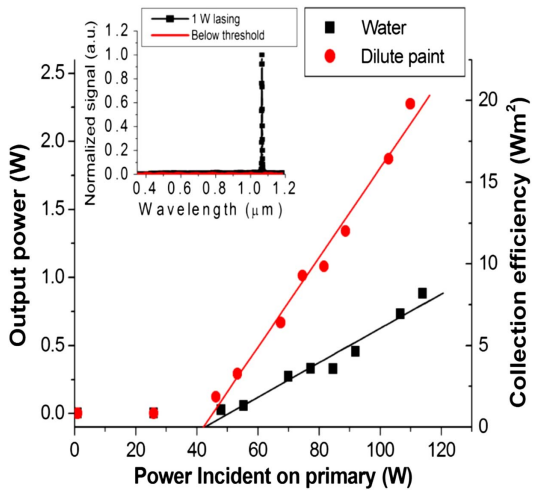

Fig. 6. (a) Laser output power (left axis) and collection efficiency (right axis) versus total solar power hitting the front surface of the Fresnel lens for both water (black squares) and water–paint (red circles) cooling liquids. (b) Spectral reading of solar pumped laser operating above the threshold (black line with squares) and below the threshold (red line).

Observations suggested that sunlight hitting the outer areas of the Fresnel lens was not contributing to sunlight entering the laser rod, implying that the primary area contributing to the laser power was smaller than the full area of the primary and that the effective collection efficiency was, therefore, higher than first thought. To test this, we inserted an aperture between the Fresnel lens and the laser rod [see inset in Fig. 5(b)] and closed it until a drop in power was observed. If we use this aperture to geometrically define our primary collection area rather than the total exposed Fresnel lens area, the effective primary concentrator area is reduced to 0.0829 m^2, and the collection efficiency increased by a factor of 1.375 to a maximum of 27.5 W/m^2 in the case of the paint–water mixture.

4. DISCUSSION

The solar laser performance achieved is significantly lower than that predicted by our modelling for the total incident solar power entering the laser rod. This indicates that our sunlight concentration system has substantial losses. We use a single fitting parameter, the efficiency of the collection optics, to fit our experimental data to our modelled data for the case of the water–white-paint mix and 98% diffuse reflectivity. This fit indicates a loss in the sunlight collection system of 70%. Figure 7 shows the modelled laser performance and the fitted experimental laser performance having accounted for this 70% loss.

To verify this loss in the collection optics, we experimentally characterized the loss found from each component; the transmission of the Fresnel lens, the focusing loss of the Fresnel lens (total power at the focus versus power transmitted through Fresnel lens), the loss from the occlusion of the high reflection (HR) laser mirror, and the loss due to overfilling of the 3 mm aperture given by the entrance diameter of the Nd:YAG laser rod. These measured losses are summarized in Table 1. A total loss of 79.3% is measured. We note that we characterized the loss from the crystal end face size using a 3 mm diameter hole in a 1 mm thick aluminum plate with a power meter behind it. The large divergence of sunlight at the focus means that light is

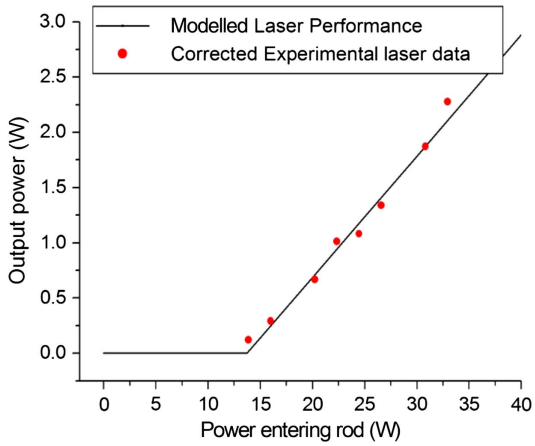

Fig. 7. Modelled (black line) and experimental (red dots) laser power as a function of power entering the laser rod accounting for the 70% loss of sunlight from the collection optics path.

Table 1. Experimentally Measured Loss from Each Component in the Sunlight Collection Path

Transmission loss of Fresnel lens	13.3%
Focusing loss of Fresnel lens	47.5%
Occlusion loss of HR laser mirror	0.9%
Loss due to overfilling of 3 mm aperture	17.6%
Total loss	79.3%

lost due to the thickness of the plate and to overfilling of the power meter. This effectively provides more loss than in the case of the Nd:YAG rod, meaning that these experimental measurements are a small overestimation of the total losses. Despite this, there is good agreement between the modelled losses and the experimentally measured losses, indicating where the greatest gains could potentially be made in future systems.

5. CONCLUSIONS

We have demonstrated a solar laser that used diffuse sunlight scattering around the laser rod in a water/white-emulsion-paint cooling and pump scattering liquid. The experimental solar laser maximum power was increased by a factor of 2.58 when the water/white paint mix was used compared to pure water alone. We model the increased absorption using ray-tracing software and use this along with a four-level laser model for Nd:YAG to identify the largest source of inefficiency in our current laser system as the losses arising from the low-cost Fresnel lens primary collector. Despite this, we reach a maximum power of 2.3 W at an irradiance of 927 W/m^2 with a collection efficiency of 20.0 W/m^2 based on our primary collection area and 27.5 W/m^2 when an iris is used to restrict the primary area without reducing laser power. In our current system, we use a single stage solar concentrator. There is significant potential to improve our laser performance using a lower loss primary without increasing complexity. An alternative would also be the use of a high quality front surface silver parabolic mirror as a primary concentrator instead of the low-cost Fresnel lens currently used. This would increase the fraction of the sunlight brought to the focus of the primary and improve the focus spot profile and size significantly. The benefits of parabolic reflectors have been demonstrated previously in solar lasers [9]. Increasing power and conversion efficiency even further could also be achieved through the use of a multistage concentration system. This is something that has been done previously in other solar laser systems [3–8], wherein a secondary non-imagine optic, for example, a compound parabolic concentrator (CPC), is placed in front of the laser medium in order to further concentrate focused incoming solar radiation form the primary concentrator.

Funding. Engineering and Physical Sciences Research Council (EPSRC) (EP/J017043/2).

REFERENCES

1. C. G. Young, "A sun-pumped CW one-watt laser," Appl. Opt. **5**, 993–997 (1966).
2. D. Liang, J. Almeida, C. R. Vistasa, and E. Guillot, "Solar-pumped Nd:YAG laser with 31.5 W/m^2 multimode and 7.9 W/m^2 TEM00-mode collection efficiencies," Solar Energy Mater. Sol. Cells **159**, 435–439 (2017).
3. M. Weksler and J. Shwartz, "Solar-pumped solid-state lasers," IEEE J. Quantum Electron. **24**, 1222–1228 (1988).
4. M. Lando, J. Kagan, B. Linyekin, and V. Dobrusin, "A solar pumped Nd:YAG laser in the high collection efficiency regime," Opt. Commun. **222**, 371–381 (2003).
5. T. Yabe, T. Ohkubo, S. Uchida, K. Yoshida, M. Nakatsuka, T. Funatsu, A. Mabuti, A. Oyama, K. Nakagawa, T. Oishi, K. Daito, B. Behgol, Y. Nakayama, M. Yoshida, S. Motokoshi, Y. Sato, and C. Baasandash, "High-efficiency and economical solar-energy-pumped laser with Fresnel lens and chromium co-doped laser medium," Appl. Phys. Lett. **90**, 261120 (2007).
6. T. H. Dinh, T. Ohkubo, T. Yabe, and H. Kuboyama, "120 watt continuous wave solar-pumped laser with a liquid light-guide lens and an Nd:YAG rod," Opt. Lett. **37**, 2670–2672 (2012).
7. D. Liang and J. Almeida, "Solar-pumped TEM00 mode Nd:YAG laser," Opt. Express **21**, 25107–25112 (2013).
8. J. Almeida, D. Liang, C. R. Vistas, and E. Guillot, "Highly efficient end-side-pumped Nd:YAG solar laser by a heliostat-parabolic mirror system," Appl. Opt. **54**, 1970–1977 (2015).
9. R. Winston, J. C. Minano, and P. Benitez, *Nonimaging Optics* (Elsevier, 2005).
10. O. Svelto, *Principles of Lasers*, 4th ed. (Springer, 1998).
11. J. Whittle and D. R. Skinner, "Transfer efficiency formula for diffusely reflecting laser pumping cavities," Appl. Opt. **5**, 1179–1182 (1966).
12. P. D. Reusswig, S. Nechayev, J. M. Scherer, G. W. Hwang, M. G. Bawendi, M. A. Baldo, and C. Rotschild, "A path to practical solar pumped lasers via radiative energy transfer," Sci. Rep. **5**, 14758 (2015).
13. S. Mizuno, H. Ito, K. Hasegawa, T. Suzuki, and Y. Ohishi, "Laser emission from a solar-pumped fiber," Opt. Express **20**, 5891–5895 (2012).
14. V. V. Datsuyk, S. Juodkazis, and H. Misawa, "Properties of a laser based on evanescent-wave amplification," J. Opt. Soc. Am. B **22**, 1471–1478 (2005).
15. I. Y. Milev, S. S. Dimov, S. Z. Kurtev, O. E. Denchev, and I. P. Angelov, "Optimization of the pumping conditions for Nd:YAG lasers," Appl. Opt. **29**, 772–776 (1990).
16. M. S. Mangir and D. A. Rockwell, "Measurements of heating and energy storage in flashlamp-pumped Nd:YAG and Nd-doped phosphate laser glasses," IEEE J. Quantum Electron. **22**, 574–580 (1986).